NASA TECHNICAL MEMORANDUM NASA-TM-76658 19820013356

NASA TM-76558

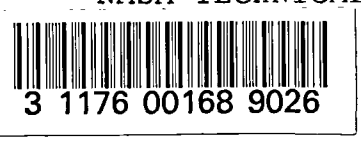

THE INFLUENCE OF A LOCAL WALL DEFORMATION ON THE DEVELOPMENT OF NATURAL INSTABILITIES IN A LAMINAR BOUNDARY LAYER

S. Burnel, P. Gougat, and F. Martin

Translation of "Influence d'une déformation locale de paroi sur le développement des instabilités naturelles d'une couche limite laminaire", Journal de Mécanique, Vol. 16, No. 3, 1977, pp. 417-439

NATIONAL AERONAUTICS AND SPACE ADMINISTRATION
WASHINGTON, D.C. 20546 JUNE 1981

ENTER:

17 1 1 RN/NASA-TM-76558
DISPLAY 17/2/1
81N27430*# ISSUE 18 PAGE 2481 CATEGORY 34 RPT#: NASA-TM-76558
CNT#: NASW-3199 81/06/00 25 PAGES UNCLASSIFIED DOCUMENT
Original language document was announced as A78-12549
UTTL: The influence of a local wall deformation on the development of natural instabilities in a laminar boundary layer
AUTH: A/BURNEL, S.; B/GOUGAT, P.; C/MARTIN, F.
CORP: National Aeronautics and Space Administration, Washington, D. C.
AVAIL.NTIS SAP: HC A02/MF A01
Transl. by Kanner (Leo) Associates, Redwood City, Calif. Original doc. prep. by Univ. of Orleans-La Source, Orleans Transl. into ENGLISH from Journal de Mecanique (France), v. 16, no. 3, 1977 p 417-439
MAJS: /*BOUNDARY LAYER TRANSITION/*DYNAMIC STRUCTURAL ANALYSIS/*LAMINAR BOUNDARY LAYER/*RESONANT FREQUENCIES/*WALL PRESSURE
MINS: / FLAT PLATES/ FLOW STABILITY/ PRESSURE DISTRIBUTION/ SPECTRUM ANALYSIS/ STABILITY TESTS
ABA: E.A.K.
ABS: The natural instabilities which propagate in the laminar boundary layer of a flat plate composed of intermittent

Technical Library
MS 185
Hampton, VA 23665

Return to Library MS-185

LRC 1 2 1176 00000 9913 A 225606371 PD
Hefner, Jerry N.
Mailstop 163
LANGLEY RESEARCH CENTER
HAMPTON, VA 23665

8/17/83 SECOND RECALL PAGE 1
Please return the following item.
If you have already done so, please disregard.

3 1176 00168 9026 8/12/83
N-151,511
Burnel, S.
Influence of a local wall deformation on the development of natur al instabilities in a laminar boundary layer.
NASA TM-76558

STANDARD TITLE PAGE

1. Report No.	2. Government Accession No.	3. Recipient's Catalog No.
NASA TM-76558		

4. Title and Subtitle	5. Report Date
THE INFLUENCE OF A LOCAL WALL DEFORMATION ON THE DEVELOPMENT OF NATURAL INSTABILITIES IN A LAMINAR BOUNDARY LAYER	June 1981
	6. Performing Organization Code

7. Author(s)	8. Performing Organization Report No.
S. Burnel (University of Orleans-La Source) and P. Gougat and F. Martin (CNRS Aerothermics Laboratory)	10. Work Unit No.

9. Performing Organization Name and Address	11. Contract or Grant No.
Leo Kanner Associates Redwood City, California 94063	NASw-3199
	13. Type of Report and Period Covered
	Translation
12. Sponsoring Agency Name and Address	14. Sponsoring Agency Code
National Aeronautics and Space Administration, Washington, D.C. 20546	

15. Supplementary Notes

Translation of "Influence d'une deformation locale de paroi sur le developpement des instabilites naturelles d'une couche limite laminaire", Journal de Mecanique, Vol. 16, No. 3, 1977, pp. 417-439.

16. Abstract

ABSTRACT.—The natural instabilities which are propagating in the laminar boundary layer of a flat plate are composed of intermittent wave trains.

A spectral analysis of these fluctuations permits to determine their frequency range where always arises a frequency f and the harmonic $2f$ only if there is a wall deformation. This analysis gives also the amplitude modulation spectrum of the instabilities. Plots of the evolution of their power spectral density are compared with the numerical results got from the resolve of the Orr-Sommerfeld equation, while the harmonic is related to a micro-recirculating flow near the wall deformation.

17. Key Words (Selected by Author(s))	18. Distribution Statement
	Unclassified-Unlimited

19. Security Classif. (of this report)	20. Security Classif. (of this page)	21. No. of Pages	22.
Unclassified	Unclassified		

THE INFLUENCE OF A LOCAL WALL DEFORMATION ON THE DEVELOPMENT OF NATURAL INSTABILITIES IN A LAMINAR BOUNDARY LAYER

S. Burnel*, P. Gougat**, and F. Martin

Abstract /417

The natural instabilities propagated in the laminar boundary layer of a flat plate are composed of intermittent wave trains.

Spectral analysis of these fluctuations can determine their frequency. There always arises a frequency f, but the harmonic 2f only appears if there is a wall deformation. Spectral analysis also gives the amplitude modulation spectrum of the instabilities. Plots of the evolution of their power-density spectrum are compared with the numerical results obtained from solution of the Orr-Sommerfeld equation, while the harmonic is related to a microflow along the wall deformation.

Introduction

In the boundary layer of a flat plate, the transition from a laminar state to a turbulent one starts with the development of unstable frequencies. This harbinger of transition has been studied by Tollmien [1] and Schlichting [2]: By introducing two-dimensional /418 velocity perturbations, defined by a current function, into the Navier-Stokes equations, the Orr-Sommerfeld equation is obtained. Its solution supplies the elements for the theory of stability: Depending on the magnitude of its reduced frequency ω^* and the Reynold's number of the flow $N_{R\delta_1}$, the perturbation introduced into the boundary layer is either amplified or attenuated by a coefficient α_i. The linear amplification in the first stages of the

*University of Orleans-La Source, Applied Mechanics and Energetics Laboratory, 45100 Orleans, France

**CNRS Aerothermics Laboratory, 4 ter, route des Gardes, 92190 Moudon, France

†Numbers in the margin indicate pagination in the foreign text.

process then gives rise to spots of turbulence whose coefficient of intermittence grows until an actual state of turbulence is reached.

It seems that the entire transition phenomenon is ruled by the development of such instabilities. The first experimental verification of this was made by Schubaure and Skramstad [3], who used a vibrating band to introduce sustained perturbations in the boundary layer. More recently, Jordinson [4] took into account the thickening of the boundary layer and studied the influence of a pressure gradient on the development of instabilities. These different comparitive studies dealt with artificial initiations of the transition phenomenon. While we have constantly used such work as a point of reference, our own study in fact concerns the influence of a wall deformation on the position of natural transition. The complexity of the phenomenon has led us to look at both the case of a wall deformation and that of a flat plate at the same time.

In the course of our study of natural instabilities, we encountered an unexpected problem -- the appearance of a harmonic of the instabilities at a right angle to the wall deformation.

2. Experimental Equipment

2.1. Wind Tunnel

Measurements were made in a subsonic wind tunnel of the Eiffel type. The test stream had a square cross section (0.5 m on a side) and a length of 1.5 m. It was preceded by a convergent nozzle with a contraction ratio of 9. The speed of the flow could vary from 4 to 30 m/sec. For speeds of between 10 and 25 m/sec, the relative level of longitudinal speed fluctuations, $\sqrt{\bar{u}'^2}/U_e$, remained basically constant and equal to 0.4%. In addition, spectral analysis of the fluctuations in the free flow speed revealed a flat spectrum without any singularity that could prematurely initiate transition. A weaker preturbulence might push transition slightly upstream without changing the structure of the phenomenon. Such a shift would not interfere at all with the comparative study of

HIGH!

/419

the development of instabilities in the presence of a wall singularity.

An incremental two-directional displacement mechanism made it possible to position hot film sensors with 0.1 mm steps in the ordinate and 1 mm ones in the abscissa.

2.2. Deformable Plate

The study was conducted in the boundary layer of a deformable flat plate. To avoid spurious vibrations, the plate was placed on four supports held by a chassis independent of the wind tunnel structure. It was preceded by an elliptical leading edge with an aspect ratio of 10. Studying the effect of a local wall deformation on the boundary layer was greatly facilitated by the machined deformable plate. The plate served as a cover for a metal frame in which three independent, sealed cavities were bored. In the lower section of each cavity were two orifices for increasing or reducing the air pressure to produce concave or convex deformations in the plate. The amplitude of the deformations was measured by a capacitive displacement pickup. The beginning of the first cavity was located at an abscissa x_o of 178 mm from the leading edge. The length λ of each cavity was 100 mm. The abscissa relative to the first cavity will be referred to as $x^* = x - x_o$. Only the first cavity was used in the present study, and we worked with constant pressures, which led to unchanging wall deformations. The amplitude of the wall deformations did not deviate by more than 10% from a sinusoidal variation of the type $y = a[1-\cos(2\pi x^*/\lambda)]$. The maximum amplitude 2a will be used to characterize the attained deformation at $x^* = \lambda/2$. Finally, note that the two-dimensional character of the deformation was conserved over 90% of its span.

2.3. Hot Film Anemometer

The measurements of average velocity and of velocity fluctuations were made with the help of an anemometric circuit. The sensitive element was either a wire or a film. The results presented here were obtained with a platimum film depositied on a quartz rod 25 μm

in diameter. We simultaneously used a split film sensor to find the direction of the velocity vector in the boundary layer. The sensor was made up of a quartz bar 150 μm in diameter and 2 mm long on which two platimum films were deposited. The plane dividing the two films was parallel to the plane of the plate. The films were controlled at constant resistance by two independent anemometric circuits. In two-dimensional flow, the ratio between the heat fluxes Φ_A and Φ_B released through convection at each film made it possible to measure the angle made by the velocity vector with the plane dividing the sensor. The sum of the heat fluxes on each film gave the magnitude of the velocity vector. /420

The sensor was adjusted through the choice of functional resistances for each film. These resistances were chosen so as to make the ratio Φ_A/Φ_B equal to one for an angle of incidence α of zero [5]. Under such conditions, for $\alpha = 90°$, the ratio Φ_A/Φ_B remained constant for speeds ranging from 5 to 16 m/sec.

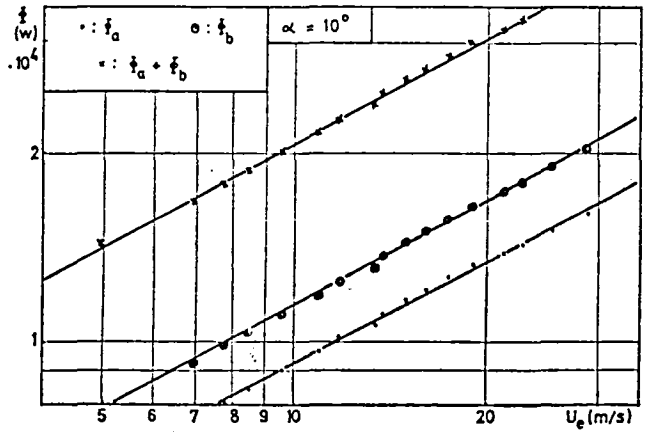

Figure 1
Exterior Flow Speed U_e vs. Total Convection Flux $\Phi_A+\Phi_B$ and also vs. the Flux of Each of the Probes Films (Φ_A and Φ_B)

We calibrated the differential probe for an angle α of 10°: It is interesting to note that the variation of the fluxes Φ_A and Φ_B followed a Collis and Williams type of power function as if only a single cylindrical film were involved. In figure 1, we have plotted the flux of each film as well as the total flux $\Phi_A + \Phi_B$. Calibration of the sensor, giving the variation of the ratio R between the fluxes Φ_A and Φ_B as a function of the angle of incidence α and the Reynolds number, has been accomplished by Olin and Kiland [6]. We adopted the following approximate independent quadratic equation to analyze the measurements: /421

$$\frac{R-R_{90}}{R_0-R_{90}}=\left(1-\frac{\alpha}{90}\right)^2,$$

with R_0 and R_{90} representing the values of the ratio R for angles α of 0° and 90°.

2.4. Frequency Analysis

The power-density spectrum of velocity fluctuations was determined by means of a real time analyzer.

The apparatus included an intake memory which received the signal in the form of a digital sample. The rate the memory was reread at was greater than the data entry rate. The signal samples' time scale was compressed before the data was fed into a heterodyne filter. This allowed the exploration of frequencies to be accelerated while at the same time maintaining a high degree of statistical precision. As an example, for an analysis ranging from 0 to 1,000 Hz, the sampling frequency would be 3,000 Hz, and the time it would take to fill up the memory would be 0.2 sec. With a time compression factor of 1,000, in 40×10^{-3} sec we would have an instantaneous analysis of 200 points with an effective resolution of 9.4 Hz. (This figure takes into account the frequency sweep and the weighting function for signal truncation effects.)

The power-density spectrum was obtained by numerical integration of a great number of instantaneous spectra. Our measurements were made by accumulating 2,048 spectra, which corresponds to a sampling time of 6 min.

The use of a tape recorder in conjunction with the real time analyzer provided us with some interesting possibilities. The velocity fluctuation signal was recorded and played back at a slower speed before being fed into the anlyzer's memory. We thus had a simultaneous oscillocope display of a portion of the instantaneous signal and of the instantaneous spectrum of this sample. The change in speed brought about by the tape recorder also enabled us to watch the signal go by and block in the memory the most

significant transient portions.

3. Influence of the Wall Deformation on the Exterior Velocity Gradient /422

3.1. Measurement of the Velocity Gradient

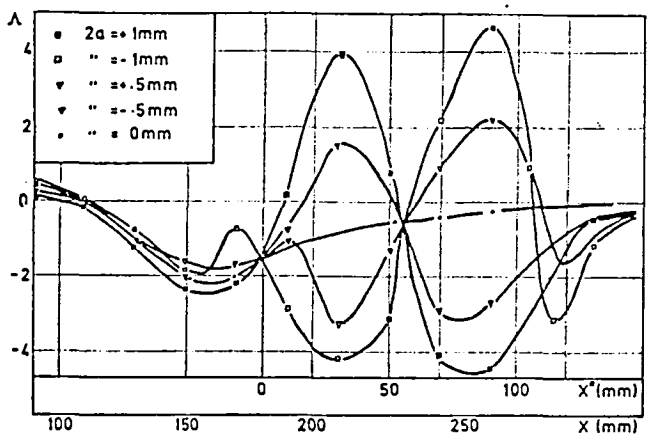

Figure 2
Polhausen Parameter Curves Showing Experimental Values Obtained as a Function of x and x* for Different Wall Deformation Amplitudes (U_∞ = 16 m/sec)

The development of the boundary layer is a function of the boundary conditions. It is therefore as necessary in flat plates as deformed ones to measure the longitudinal velocity gradient at the edge of the free flow boundary layer. The results are presented in figure 2, where the gradient is characterized by the value of the Polhausen parameter $\Lambda = (\delta^2/\nu)(dU_e/dx)$. The experimental curves intersect at x* = 0 and x* = 50 mm. This result is explainable when the deformation's profile is sinusoidal. The potential flow along the profile is then of the form:

$$\frac{U_e}{U_r} = 1 + \frac{2\pi a}{\lambda} e^{-2\pi y/\lambda} \cos\frac{2\pi x^*}{\lambda},$$

from which

$$\Lambda = K_a e^{-2\pi y/\lambda} \sin\frac{2\pi x^*}{\lambda},$$

which corresponds to a bundle of curves cutting the $\Lambda = 0$ axis at the points $x^* = 0$, $x^* = \lambda/2$, and $x^* = \lambda$. The experimental curve bundle differed slightly from this because the deformation of the plate had a finite length λ. In addition, the elliptical leading /423 edge induced a velocity gradient which modified the potential flow expression.

3.2. Transition Position

Previous experimental work showed that the phenomenon of transition on a flat plate is not characterized with enough precision by the evolution of the average velocity profile, which gradually changes from a Blasius profile to a turbulent one [7]. In contrast, the study of how longitudinal fluctuations develop provided a "transition criterion" that was a little more precise.

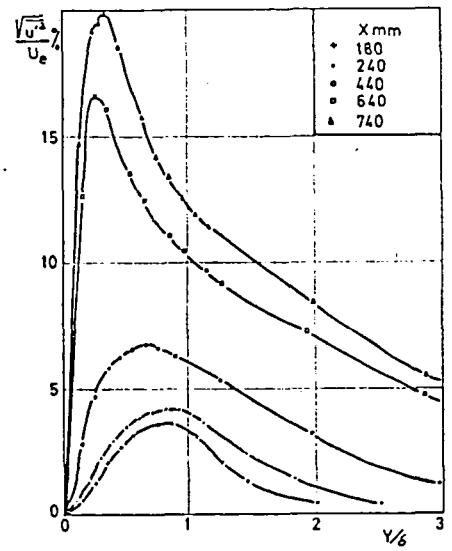

Figure 3
Velocity Fluctuation Rate vs. Ordinate on a Flat Plate for Various Abscissas (U_∞ = 12.5 m/sec)

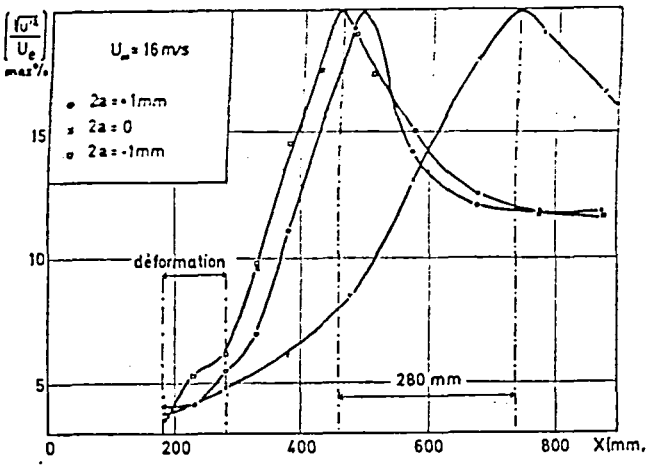

Figure 4
Influence of the Wall Deformation on Transition Position (U_∞ = 16 m/sec)

In figure 3, we show how the $\sqrt{\overline{u'^2}}/U_e$ level changes as a function of the ordinate for various abscissas. Both the maximum value of $\sqrt{\overline{u'^2}}/U_e$ and the ordinate at which it is achieved depend on the abscissa. To avoid the difficulties of a three-dimensional representation ($\sqrt{\overline{u'^2}}/U_e = f(x,y)$), we have characterized each of the $\sqrt{\overline{u'^2}}/U_e = f(y)$ curves by the value of its maximum, which we have labled $(\sqrt{\overline{u'^2}}/U_e)_{max}$.

The variation of the quantity $(\sqrt{\overline{u'^2}}/U_e)_{max}$ as a function of the abscissa is presented in figure 4 for both the flat plate and

two different wall deformation amplitudes. These curves have in turn a maximum whose abscissa could be adopted as the criterion for transition. /424

Thus, a negative wall deformation with a -1 mm amplitude causes transition to shift forward by 37%. Note that there is only a 3% difference between the forward shift due to positive deformations (+1 mm) and negative ones (-1 mm).

In fact, the abscissas at which this criterion is applied correspond to states of transition which are already advanced, and the overall measurements only illustrate the significant effect a wall deformation of small amplitude has on the phenomenon.

In order to study pretransitional mechanisms, we had to investigate the detailed structure of the instantaneous signal in the zone where the Reynolds number was close to the critical value. This enabled us to discover the frequency range of the natural instabilities and their coefficient of amplification.

4. Observation of the Velocity Fluctuation Signal

4.1. Elimination of Low Frequencies

Oscilloscopic observation of the instantaneous signal showed the existence of low frequencies (below 200 Hz). We attempted to describe the changes in the effective value of such frequencies. They were present from the leading edge onward and existed in the laminar zone. /425 Their variation as a function of the abscissa did not seem to exhibit any distinguishing feature. It seemed possible to explain them by the unstable position of the stop point on the leading edge.

We will limit ourselves to mentioning their existence. In so far as the low frequencies did not appear to influence transition, the rest of the study used a filtered instantaneous signal.

4.2. Integrated Spectra

Thus, after filtering out the low frequencies, the velocity fluctuation signal was fed into the analyzer. The signals' power-density spectrum is presented in figure 5 for an abscissa $x^* = 50$ mm and an ordinate $y = 0.1$ mm, which is where the signal to noise ratio was the best:

-- Case a refers to a flat plate. The frequency ranges from 300 to 700 Hz, and, for a Reynolds number of 630, the maximum energy level within this range is located at the frequency $f_1 =$ 500 Hz.

-- Case b refers to a deformed plate. In addition to the energy contribution at 500 Hz, a second maximum is located at $f_2 =$ 1,000 Hz for the Reynolds number under consideration.

4.3. Instantaneous Signals and Their Spectra

Detailed observation of the instantaneous signals was obtained with the aid of the real time analyzer after speed reduction by means of a tape recorder. The instantaneous signal sample was put in the memory and then analyzed. Simultaneous displays of the instantaneous signals and of their spectra are shown in figure 5:

-- Case c corresponds to a signal sample obtained on a flat plate: The instantaneous signal was a relatively pure sinusoid, modulated in amplitude. The instantaneous spectrum, like the integrated one, exhibits a maximum energy level at a frequency of 500 Hz.

-- Cases d, e, and f correspond to three samples involving deformed plates. The instantaneous signals were no longer pure sinusoids. For cases d and e, the instantaneous spectra simultaneously exhibit a frequency f_1 of 500 Hz and a frequency f_2 of 1,000 Hz. In contrast, case f's spectrum only exhibits the 1,000 Hz f_2 frequency.

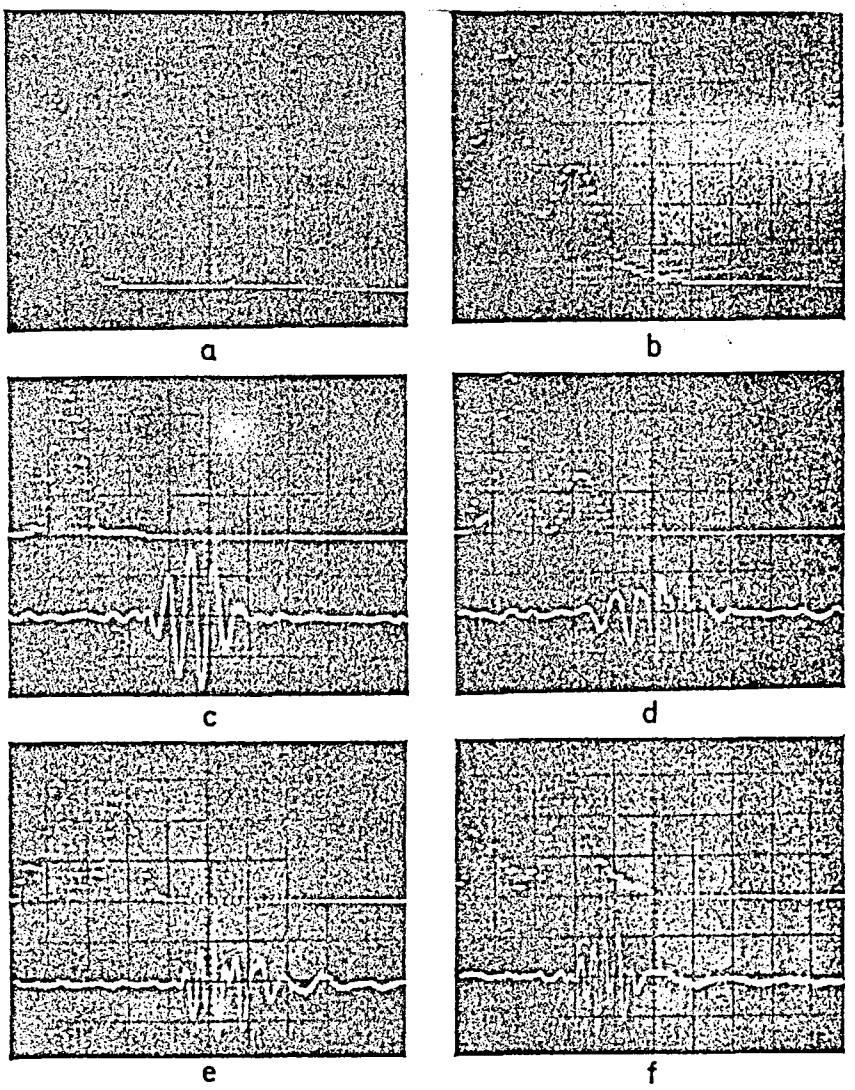

Figure 5
Integrated Spectra of a Portion of the Signal Obtained:
a) Flat Plate, 2a = 0, at x* = 50 mm and y = 0.1 mm
b) Deformed Plate, 2a = -1, at x* = 50 mm and y = 0.1 mm
Unstable Bursts Characteristic of the Hot Wire Signals and their Instantaneous Spectra (U_∞ = 16 m/sec):
c) Flat Plate; d,e,f) Deformed Plate

The structures of instantaneous signals obtained with a flat plate and with deformed ones were similar. In both cases, the fundamental frequency appeared in the form of intermittent wave trains. In deformed plates, the fundamental was altered by a harmonic, but its structure remained the same (frequency, intermittent character). /427

4.4. Identification of the Harmonic

The signal samples reproduced in figure 5 show that the f_2

frequencies were twice those of f_1. The harmonic of the instabilities was thus involved here. (Note that only the first harmonic existed.) This was confirmed for other free flow speeds and other abscissas: When the Reynolds number was changed, the f_1 frequency varied, but the f_2 frequency remained double f_1. What is more, examination of the instantaneous signals in figure 5 shows that the energy present in the spectrum at f_2 is due to a perturbation grafted on to the sinusoid of frequency f_1. The fact that only the first harmonic existed eliminates the proposition that the electronic signal processing circuits were saturated. For the same amplitude wall deformation and for a given sensor position, all the samples were not contaminated in the same way by the f_2 frequency. In particular, we see in figure 5 that the contribution of f_2 was greater in sample e than in sample d. Sometimes the f_1 frequency disappeared completely to the benefit of frequency f_2. This was the case in sample f.

4.5. Identification of the Fundamental Frequency

Obremski's and Morkovin's theoretical results [8] concern solving the Orr-Sommerfeld equation so as to trace the equal amplification curves in the ω^*, $N_{R\delta_1}$ plane for the case of a spatial variation in the instabilities. At a given Reynolds number, it is possible to calculate the range of unstable frequencies having maximum amplification.

The experimental results concerning the f_1 frequency on a flat plate for different Reynolds numbers were in good agreement with the theoretical ones (figure 6). However, it is interesting to return to the instantaneous signal samples of figure 5 in order to note that the period of the phenomenon seems constant although the analysis resulted in a wide spectrum around f_1. We have tried to interpret this phenomenon in terms of amplitude modulation. The details are given in figure 7. Let us start with a section of the instantaneous signal (figure 7a) and its spectrum (figure 7a') and look for an analogy with a simple model of a pure sunsoid of frequency f whose amplitude is modulated by a low frequency f' (figure 7b). The /428

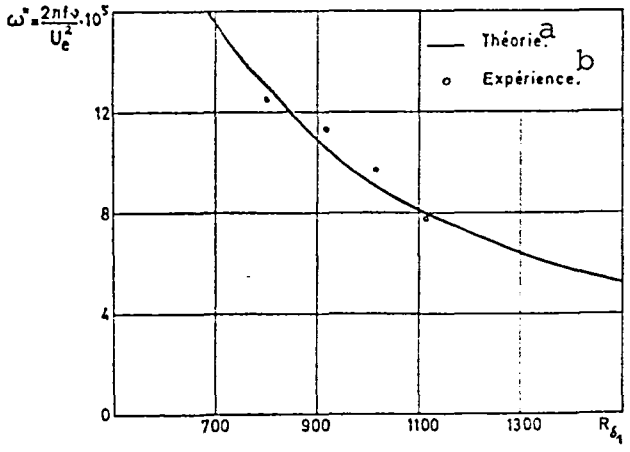

Figure 6
Frequency vs. Reynolds Number in Relation to Thickness of Boundary Layer Displacement
$N_{R\delta 1} = U_\infty \delta_1 / \nu$
———, Theoretical Maximum Amplification Curve
O, Experimental Points
$2a = 0$

Key: a) Theory
b) Experiment

spectrum shows a line at frequency f and two modulation lines at f ± f' (figure 7b'). The conventional approach in signal processing for isolating the f' frequency is to carry out a full wave rectification of the signal (figure 7c). The spectrum of the rectified signal includes a line at a frequency of 2f, two modulation lines at 2f ± 2f', and at all the higher harmonics as well, and finally a line at f' (figure 7c'). The model can in fact allow for modulation by narrow band noise (figures 7d and 7d'), and rectification would result in isolating a continuous modulation spectrum (figures 7e and e'). The same procedure of full wave rectification could be applied to the sample of the physical signal (figure 7f). Analysis of the rectified signal uncovers a whole range of low frequencies constituting a continuous modulation spectrum (figure 7f'). We can thus explain why the instantaneous signal samples were made up of pure sinusoids while their spectra only contained a single line. In fact, it is difficult at the present state of signal processing to decide on the origin of the modulation spectrum: Two phenomena are simultaneously at play, the actual modualtion of the unstable bursts /430 and the intermittence function for these bursts. We have hypothesized that these two phenomena are provoked by the low frequencies present in the boundary layer, but the correlation between the modulation spectrum and the spectrum of low frequencies cannot be documented except by modifying the low frequencies' power-density spectrum.

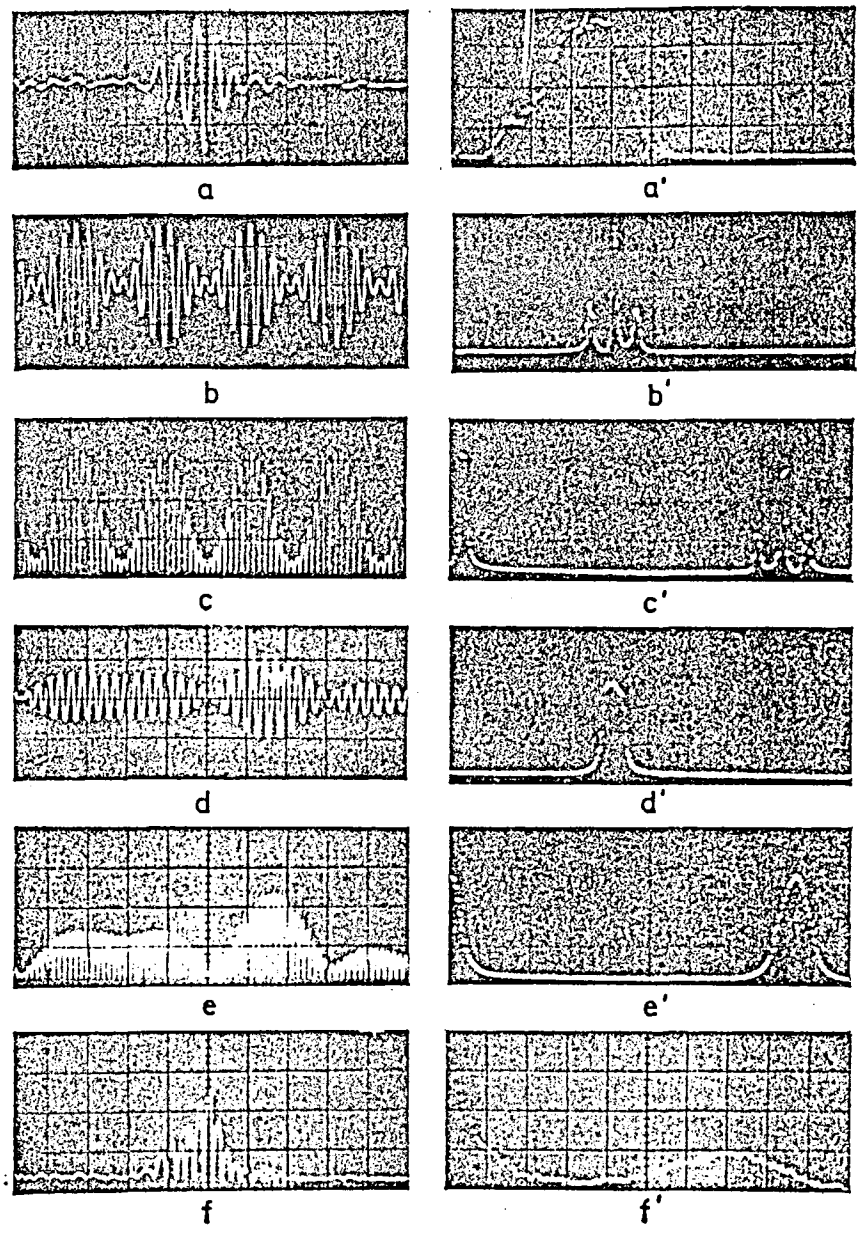

Figure 7
Amplitude Modulation by a Low Frequency Spectrum
Time Scale: 8 x 10^{-3} sec/square for Instantaneous Signals,
100 Hz/square for Spectra
a) Unstable Burst on a Flat Plate for a Reynolds Number of 1110
b) Sinusoid with Amplitude Modulation
c) Signal b after Full Wave Rectification
d) Sinusoid Modulated by Narrow Band Noise
e) Signal d after Full Wave Rectification
f) Unstable Burst in a after Full Wave Rectification
a',b',c',d',e', f': Spectra of Signals a,b,c,d,e,f, Respectively

5. Measurement of Energy for the Fundamental Frequency

5.1. Variation as a Function of the Ordinate

We have now established that for a given Reynolds number, the instabilities have a fixed frequency f_1 and that this frequency corresponds to the power-density spectrum maximum for the velocity fluctuations in the range of analysis under consideration. We will designate the energy contribution made by the fluctuations of frequency f_1 as $(\sqrt{\overline{u'^2}}/U_e)_{f_1}$.

We will only examine the variation in this quantity at a single abscissa (x* = 100 mm), and only for two deformation amplitudes (2a = +1 mm and 2a = -0.5 mm), but the phenomenon is of the same type for a flat plate.

Case of the Positive Deformation 2a = +1 mm

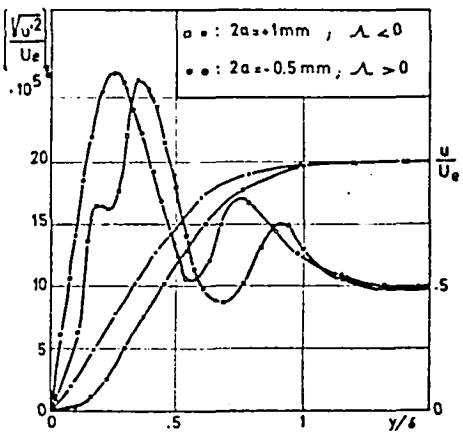

Figure 8
Energy of f_1 Instabilities vs. y/δ and Profiles of Corresponding Average Speeds
U_∞ = 16 m/sec, x*=100 mm
δ_B=2.51, $N_{R\delta_1}$=937

The variation in energy at frequency f_1 as a function of y/δ is shown in figure 8. A first maximum exists at y/δ = 0.18. This maximum can be attributed to the presence of a point of inflection in the average velocity profile. According to Karman-Pohlhausen, the velocity profile can be represented by a fourth order polynomial approximation in y/δ. The polynomial's coefficients depend on the parameter Λ, characteristic of the exterior velocity gradient. The point of inflection on the velocity profile $(d^2(U/U_e)/d(y/\delta)^2 = 0)$ is obtained for $y/\delta = -\Lambda/(12-2\Lambda)$. For our experimental conditions, x* = 100 mm, 2a = +1 mm, one finds that $\Lambda = -3.5$ and thus $y/\delta = 0.184$, which is little different than the ordinate of the first maximum. This correlation between the amplification of

of the instabilities and the point of inflection on the velocity profile was proposed by Tollmien to be a singularity of the Orr-Sommerfeld equation.

The second maximum occurs at $y/\delta = 0.35$, which is in good agreement with the experimental results of Ross, Barnes, and Burns [9]. Note that not only the value of this maximum, but also its ordinate in the boundary layer varies as a function of the Reynold's number. However, in all cases the maximum's ordinate is such that the average speed at this point is $U/U_e = 0.4$, which corresponds to another singularity in the Orr-Sommerfeld equation, at which the velocity is equal to the phase velocity of the instabilities. Thus, it is the value of the maximum that is useful to us in characterizing the state of instability amplification at a given abscissa. /431

A third maximum exists in the neighborhood of the boundary layer's edge. We do not attach any importance to this maximum because it concerns an input of energy at the f_1 frequency resulting from the general return of the spectrum to the continuous spectrum of free flow.

Case of the Negative Deformation 2a = -0.5 mm

The results are presented in figure 8.

There is no point of inflection on the average velocity profile and therefore no first maximum at $y/\delta = 0.2$. This is due to the fact that for the abscissa and deformation under consideration, the Λ parameter is positive.

The maximum energy level is located at the point where the speed $U/U_e = 0.4$.

Thus, the variation of the power-density spectra of the f_1 instabilities along the normal to the wall depends on the sign of the exterior velocity gradient. However, the variation exhibits an extremum characteristic of the state of instability amplification /432

in both cases presented here. We can now justify the choice of these two deformation amplitudes for figure 8. We chose a positive and a negative amplitude leading to the same state of amplification at x* = 100 mm. We thus showed that the existence of a first maximum is independant of the state of instability amplification and depends only on the presence of a point of inflection on the velocity profile.

5.2. Variation as a Function of the Abscissa

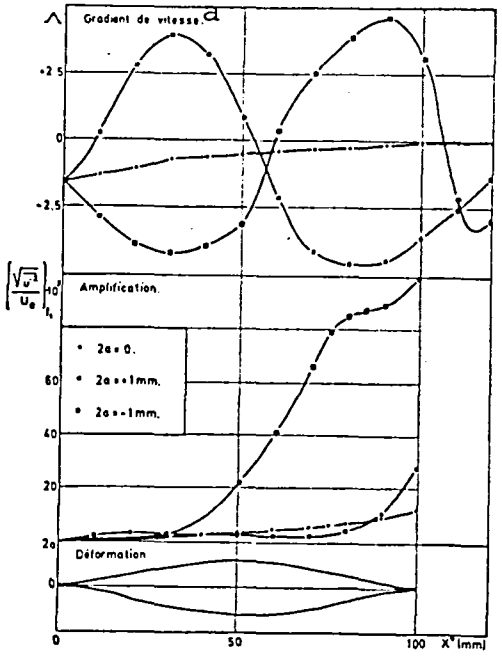

Figure 9
Amplification Coefficients of f_1 Instabilities vs. Exterior Velocity Gradient (U_∞ = 16 m/sec)

Key: a) Velocity Gradient

The variation of the maximum level of instability as a function of the abscissa is traced in figure 9. The curves in the figure express the spatial amplification of the instabilities for a flat plate and for two different deformation amplitudes.

The amplification curve for the flat plate is monotonic:

Its slope represents the amplification factor. For an abscissa x* = 50 mm corresponding to a Reynolds number $N_{R\delta_1}$ = 870, the experimental amplification coefficient $-\alpha_i \delta_1 / N_{R\delta_1}$ at the reduced frequency $\omega^* = 1.2 \times 10^{-4}$ equaled 2.1×10^{-5} and did not differ by more than 3% from the the theoretical value obtained from the Obremski-Morkovin tables.

The curves for the defomable wall exhibit localized changes in curvature at abscissas which depend on the sign of the deformation:

-- For a positive deformation, the favorable gradient ($\Lambda > 0$) intervenes at the beginning of the amplification and attenuates the

instabilities. Their energy level at $x^* = 60$ mm is less than at $x^* = 30$ mm.

-- For a negative deformation, the instabilities are already greatly amplified by the time the favorable gradient ($\Lambda > 0$) intervenes. The gradient can only reduce the amplification very slightly and does not succeed in attenuating the instabilities.

The amplification curves in figure 9 are not traced beyond the abscissa $x^* = 100$ because in the presence of a wall deformation of either sign, the unstable bursts exhibit a wide spectrum corresponding to a complete breakup, and it becomes impossible to characterize the evolution of transition by the selective amplification of one unstable frequency.

At a right angle to the deformation in a given section, the /433
effect of the exterior velocity gradient depends on the energy level attained by the instabilities in the section. There is therefore no direct corrspondence between the state of amplification and the local value of the Λ parameter.

6. Energy Measurement for the Harmonic

6.1. Variation as a Function of the Ordinate

In figure 10 we have plotted the relationship between y/δ and the energy level of the fluctuations in relative velocity at a frequency f, i.e. the quantity $(\sqrt{\overline{u'^2}}/U_e)_f$ for frequencies f_1 (curve a) and f_2 (curve b). These values were obtained for a wall deformation amplitude $2a = -1$ mm and an abscissa $x^* = 50$ mm. Curve b shows that the unstable frequency f_2 had maximum energy at a reduced ordinate y/δ of 0.1, which corresponds to a small distance from the wall (between 0.1 and 0.2 mm). Curve c represents the /434
variation as a function of y/δ of the ratio $(\sqrt{\overline{u'^2}}/U_e)_{f_2}/(\sqrt{\overline{u'^2}}/U_e)_{f_1}$, which was at its maximum near the wall, attaining there a value on the order of 55% and decreasing very rapidly with increasing distance since the f_1 frequency was dominant.

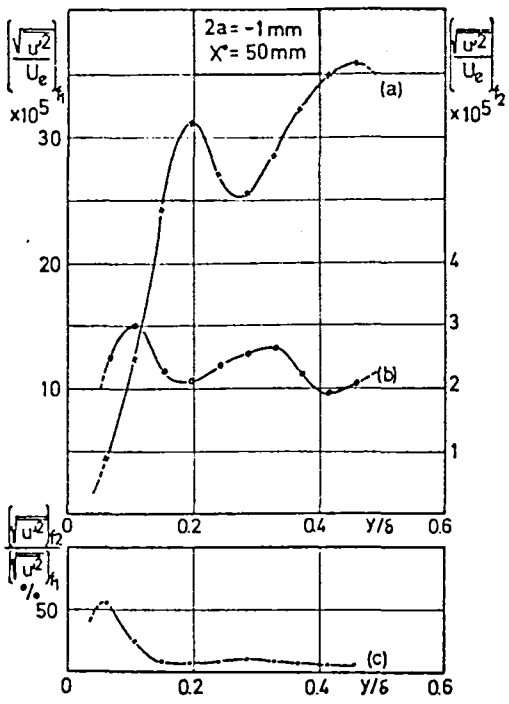

Figure 10
Ordinate Dependency of Energy of Instabilities at Frequencies f_1 (a) and f_2 (b) and of the Harmonic Rate (c)
U_∞=16 m/sec, 2a=-1 mm, x*=50 mm, δ_B=2.27

We were especially interested in the maximum energy level for frequency f_2 and in the maximum value of the energy ratio between the two frequencies.

6.2. Variation as a Function of the Abscissa

The set of curves in figure 11 represents the dependence of maximum energy, i.e. the quantity $(\sqrt{\overline{u'^2}}/U_e)_{f_2 max}$, on x* for various deformation amplitudes. Notice that the greater the amplitude of the deformation, the more visible the phenomenon was. Note also that the curves have a maximum at an abscissa x* of between 50 and 70 mm, depending on the deformation amplitude, and therefore downstream from the middle of the cavity. /435

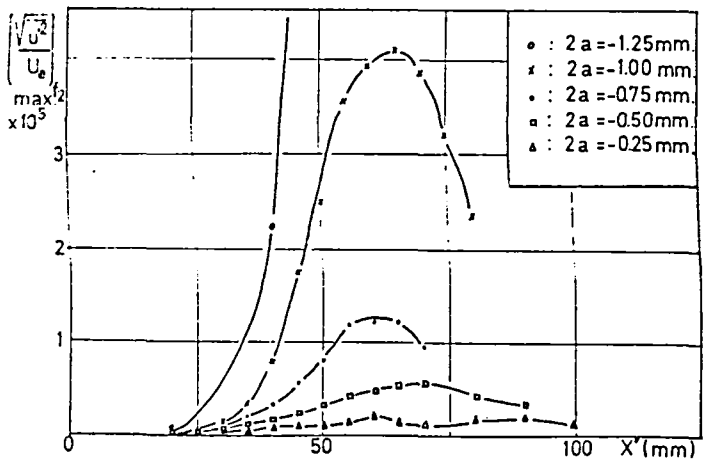

Figure 11
Energy of Instabilities of Frequency f_2 vs. Abscissa for Various Wall Deformation Amplitudes (U_∞=16m/sec)

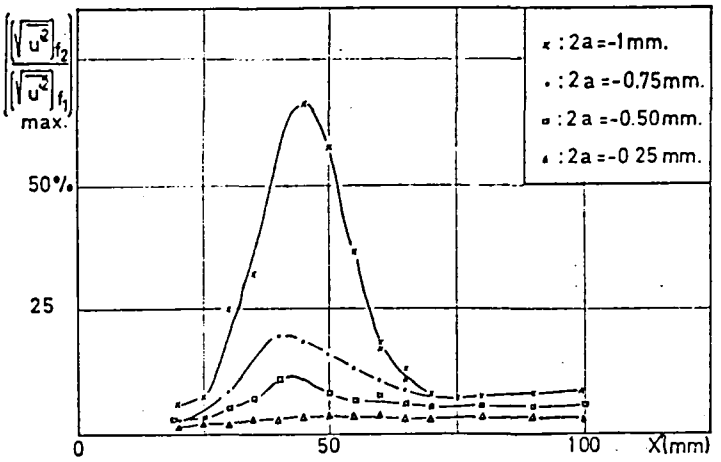

Figure 12
Harmonic Rate vs. Abscissa
(U_∞ = 16 m/sec)

On the contrary, curves representing the variation of the maximum ratio between the two energies as a function of x* (figure 12) attain a maximum for abscissas of between 40 and 60 mm, and therefore upstream from the middle of the cavity. The curves then rapidly tend toward horizontal asymptotes. /436

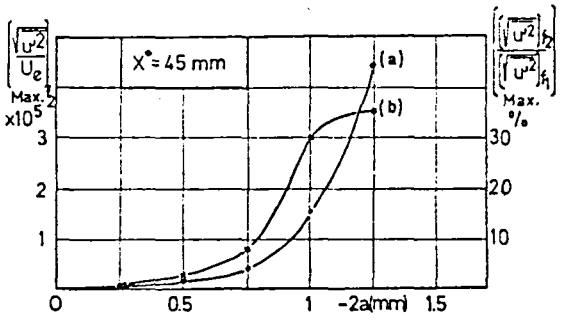

Figure 13
Dependence of Energy of Instabilities at f_2 (a) and of Harmonic Rate (b) on Wall Deformation Amplitude (2a) at x*=45 mm
U_∞ = 16 m/sec

In figure 13, we have plotted the curves showing the dependence on amplitude 2a of maximum energy at frequency f_2 (curve a) and of the maximum energy ratio between the two frequencies (curve b). The latter curve exhibits a change in curvature between -0.75 and -1 mm, which does not exist on curve a. This clearly shows the difference in behavior between frequency f_2 and the f_1-f_2 energy ratio.

6.3. Discussion of the Harmonic's Origin

On the basis of these experimental results, various proposals could be advanced to explain the harmonic's origin.

We have already eliminated the hypothesis of a distortion arising in the processing of the hot wire signal, but it remains possible that the physical phenomenon itself is nonlinear. This would result in the propogation of harmonics.

However, this proposition does not seem plausible when the harmonic ratio attains values as high as 50%. Furthermore, let us go back to figure 12 and consider for example the variation in the harmonic ratio between x* = 50 mm and 60 mm for a -1 mm wall deformation. We find the following values:

	$x^* = 50$ mm	$x^* = 60$ mm
$(\sqrt{\overline{u'^2}}/U_e)_{f_1}$	$4.96.10^{-5}$	$22.4.10^{-5}$
$(\sqrt{\overline{u'^2}}/U_e)_{f_2}$	$2.6.10^{-5}$	$3.6.10^{-5}$
$(\sqrt{\overline{u'^2}}/U_e)_{f_2}/(\sqrt{\overline{u'^2}}/U_e)_{f_1}$	52%	16,2%

These values show that while the fundamental frequency is amplified by a factor of about 4, the harmonic ratio diminishes by 2/3. This is not compatible with the hypothesis linking the presence of the instabilities' first harmonic to the nonlinear character of their development. If a nonlinear phenomenon were in fact involved, the harmonic ratio would increase in a continuous manner when the fundamental frequency was amplified. /437

If in contrast we look at the geographic location of the region where the harmonic existed, we observe that the zone where the harmonic ratio was greatest corresponds to the zone where the exterior velocity gradient was the most negative.

For a zero gradient, we have seen (figure 6) that the f_1 frequency corresponded to the frequency having maximum amplification according to stability theory. Now, a negative gradient provoked a widening of the range of unstable frequencies and if the gradient was sufficiently negative, the f_2 frequency fell in the unstable area.

To give an example, for the abscissa x* = 50 mm, corresponding in a flat plate ($\Lambda = 0$) to $N_{R\delta_1} = 850$, the frequency with maximum amplification had a reduced pulsatance ω^* of 1.1×10^{-4}. In contrast, in the conditions of flow ($\Lambda = -12$) the pulsatance corresponding to the harmonic, $\omega^* = 2 \times 10^{-4}$, had maximum amplification, and the fundamental was located in the unstable area. The ratio of about 2 between the two pulsatances led us to make the hypothesis that the harmonic encountered in the experiments was due to a laminar microflow along the deformation.

We then used the split film sensor to measure the velocity vector's angles of incidence in the boundary layer. Figure 14 /438

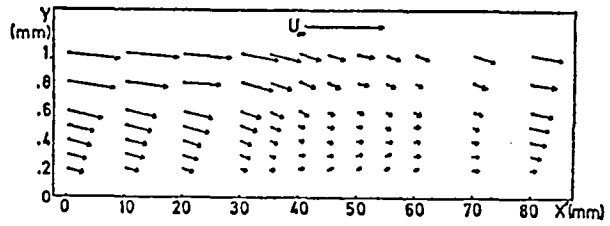

Figure 14
Representation of Velocity Vector in the Wall Deformation Zone, 2a = -1 mm
(U_∞ = 16 m/sec)

depicts the velocity vector along the deformation (magnitude and direction). There did not appear to be any return flow in the neighborhood of the wall. There were, of course, strongly perturbed zones, but the velocity vector's angle of incidence always remained relatively small.

Under these conditions, we rejected the hypothesis of a permanent flow as the origin of the f_2 frequency. However, observation of the instantaneous signal showed us the intermittent character of f_2's appearance in the unstable bursts. This led us to readjust our hypothesis by proposing that the f_2 frequency could be due to an intermittent flow [10]. The absence of a threshold in the variation of the harmonic and the harmonic ratio with deformation amplitude (figure 13) could then be explained by a gradual increase in the intermittence of the microflow.

7. Conclusion

The natural instabilities which arise in a flat plate's laminar boundary layer are composed of intermittent wave trains. Spectral analysis of these fluctuations localized their frequencies and allowed us to isolate their amplitude modulation spectrum. Although there is a fundamental difference between natural instabilities and those under consideration in Tollmien's and Schlichting's theoretical calculations, the frequencies of the instabilities and their amplification coefficients were identical to those predicted by stability theory. A wall deformation does not change the structure of the phenomenon. It only induces an exterior velocity gradient which, according to its sign, either amplifies or attenuates the instabilities to a degree depending on their energy level. Observation of the instantaneous velocity fluctuation signal as well as

spectral analysis showed that in a zone of negative gradient the first harmonic of the instabilities appears in the form of a perturbation grafted onto the unstable bursts of frequency f_1.

Given the significance of the harmonic under certain experimental conditions, its existence could not be satisfactorily explained by a nonlinear characterization of the phenomenon.

We also eliminated the hypothesis of a permanent microflow being at the origin of the perturbation at frequency f_2. In contrast, the intermittent character of this perturbation is an indication that it might be due to a microflow that is itself intermittent. /439 Such a phenomenon could not be detected by the split film anemometer sensor, which only provided average values for the velocity's angle of incidence.

Apart from the instantaneous signals and their spectra, all the measurements we have presented correspond to temporal averages. This gives the study a generalized character. The problematic intermittence of the instabilities makes a statistical analysis of the phenomenon necessary, in fact. We will thus attempt to restructure the boundary layer by imposing a definite, known artificial intermittence on it. To do this, we are investigating the influence of sinusoidal wall vibrations on the boundary layer.

(Manuscript received October 30, 1975, revised February 22, 1977.)

REFERENCES

[1] Tollmien, L., "General Instability Criterion of Laminar Velocity Distributions", TM 792, NACA, 1936.

[2] Schlichting, H., Boundary Layer Theory, McGraw-Hill, 1968.

[3] Schubauer, G.B. and H.K. Skramstad, "Laminar Boundary Layer Oscillations and Transition on a Flat Plate", TR 909, NACA, 1948.

[4] Jordinson, R., "Numerical Integration of the Orr-Sommerfeld Equation", J. Fluid Mech., 43/4, 801-811 (1970).

[5] Gougat, P. and F. Martin, "Etude d'une sonde différentielle à deux films chauds" [Study of a Split Hot Film Differential Sensor], C.R. Acad. Sc., 277, series A, 1123-1126 (1973).

[6] Olin, J.G. and R.B. Kiland, "Split Film Anemometer Sensor for Three Dimensional Velocity Vector Measurement", Symposium on Aircraft Wake Turbulence, Seattle, September 1970.

[7] Burnel, S., Influence d'un gradient de vitesse sur l'amplification des fréquences naturelles dans une couche limite [Influence of a Velocity Gradient on the Amplification of Natural Frequencies in a Boundary Layer], Thesis for the Third Cycle, University of Paris VI, 1972.

[8] Obremski, H.J., M.V. Morkovin, and M. Landhal, "A Portfolio of Stability Characteristics of Incompressible Boundary Layers", AGARDograph. 134, 1969.

[9] Ross, J.A., F.H. Barnes, J.G. Burns, and M.A.S. Ross, "The Flat Plate Boundary Layer: Comparison of Theory with Experiment", J. Fluid Mech., 43, part 4, 819-832 (1970).

[10] Martin, F., Etude d'instabilités naturelles de fréquence non prévue par la théorie de la stabilité dans une couche limite laminaire [Study of Natural Frequency Instabilities Unpredicted by Stability Theory in a Laminar Boundary Layer], Thesis for the Third Cycle, University of Paris VI, 1973.